

MHFC: Multi-Head Feature Collaboration for Few-Shot Learning

Shuai Shao^{†,1}, Lei Xing^{†,2}, Yan Wang³, Rui Xu¹, Chunyan Zhao⁴, Yanjiang Wang^{*,1}, Baodi Liu^{*,1}

¹College of Control Science and Engineering, China University of Petroleum (East China)

²College of Oceanography and Space Informatics, China University of Petroleum (East China)

³Beihang University

⁴Suzhou Centennial College

shuaishao@s.upc.edu.cn, upc_xl@163.com, wangyan9509@gmail.com, ruixu@s.upc.edu.cn

zhaocy@scc.edu.cn, yjwang@upc.edu.cn, thu.liubaodi@gmail.com

ABSTRACT

Few-shot learning (FSL) aims to address the data-scarce problem. A standard FSL framework is composed of two components: (1) Pre-train. Employ the base data to generate a CNN-based feature extraction model (FEM). (2) Meta-test. Apply the trained FEM to acquire the novel data's features and recognize them. FSL relies heavily on the design of the FEM. However, various FEMs have distinct emphases. For example, several may focus more attention on the contour information, whereas others may lay particular emphasis on the texture information. The single-head feature is only a one-sided representation of the sample. Besides the negative influence of cross-domain (e.g., the trained FEM can not adapt to the novel class flawlessly), the distribution of novel data may have a certain degree of deviation compared with the ground truth distribution, which is dubbed as distribution-shift-problem (DSP). To address the DSP, we propose **Multi-Head Feature Collaboration (MHFC)** algorithm, which attempts to project the multi-head features (e.g., multiple features extracted from a variety of FEMs) to a unified space and fuse them to capture more discriminative information. Typically, first, we introduce a subspace learning method to transform the multi-head features to aligned low-dimensional representations. It corrects the DSP via learning the feature with more powerful discrimination and overcomes the problem of inconsistent measurement scales from different head features. Then, we design an attention block to update combination weights for each head feature automatically. It comprehensively considers the contribution of various perspectives and further improves the discrimination of features. We evaluate the proposed method on five benchmark datasets (including cross-domain experiments) and achieve significant improvements of 2.1%-7.8% compared with state-of-the-arts.

CCS CONCEPTS

• **Computing methodologies** → **Image representations**; **Object identification**.

[†] indicates equal contribution. * indicates corresponding author.

Permission to make digital or hard copies of all or part of this work for personal or classroom use is granted without fee provided that copies are not made or distributed for profit or commercial advantage and that copies bear this notice and the full citation on the first page. Copyrights for components of this work owned by others than ACM must be honored. Abstracting with credit is permitted. To copy otherwise, or republish, to post on servers or to redistribute to lists, requires prior specific permission and/or a fee. Request permissions from permissions@acm.org.

MM '21, October 20–24, 2021, Virtual Event, China

© 2021 Association for Computing Machinery.

ACM ISBN 978-1-4503-8651-7/21/10...\$15.00

<https://doi.org/10.1145/3474085.3475553>

KEYWORDS

Multi-head feature collaboration (MHFC); few-shot learning (FSL); distribution-shift-problem (DSP); subspace learning

ACM Reference Format:

Shuai Shao^{†,1}, Lei Xing^{†,2}, Yan Wang³, Rui Xu¹, Chunyan Zhao⁴, Yanjiang Wang^{*,1}, Baodi Liu^{*,1}. 2021. MHFC: Multi-Head Feature Collaboration for Few-Shot Learning. In *Proceedings of the 29th ACM International Conference on Multimedia (MM '21)*, October 20–24, 2021, Virtual Event, China. ACM, New York, NY, USA, 14 pages. <https://doi.org/10.1145/3474085.3475553>

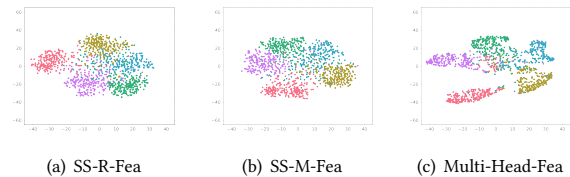


Figure 1: t-SNE visualization of features on mini-ImageNet. "SS-R-Fea" and "SS-M-Fea" indicate two categories of different single-head features (for the details, please refer to Section 4.4). "Multi-Head-Fea" denotes the fusion feature after the proposed MHFC. Multi-Head-Fea based distribution is more helpful to classification tasks.

1 INTRODUCTION

Machine learning has help machines achieve outstanding performances in computer vision tasks, such as person re-identification [8, 45, 46], image classification [17, 35, 50]. One indispensable factor is attributed to the large-scale labeled data. However, as the limitation of actual circumstances, it may be infeasible to collect large amounts of labeled data in the real world. Thus, few-shot learning (FSL) has attracted growing attention recent year. It targets to help machines achieve or even surpass human beings' level with scarce labeled samples. Generally, in FSL-based classification tasks, the current popular model usually includes two components: (1) Pre-train. Employ the base data \mathcal{D}_{base} to generate a convolutional neural network (CNN) based feature extraction model (FEM). (2) Meta-test. First, extract the features of novel data $\mathcal{D}_{novel} = \{\mathcal{S}, \mathcal{U}, \mathcal{Q}\}$, where \mathcal{S} , \mathcal{U} and \mathcal{Q} denote support set, unlabeled set and query set. Next, design a classifier to recognize the query samples \mathcal{Q} . Notably,

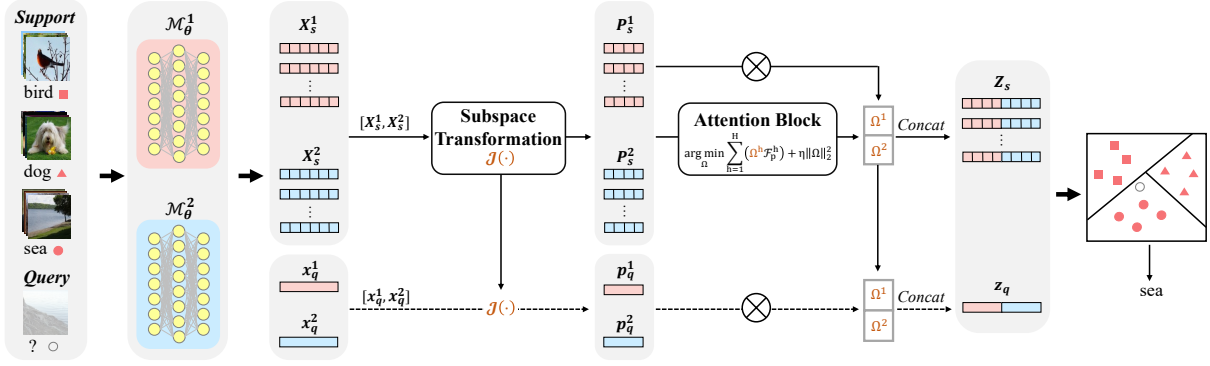


Figure 2: The framework of MHFC on inductive few-shot learning (IFSL). Assume we have two heads of feature extraction models (FEMs), e.g., \mathcal{M}_θ^h , where $h = [1, 2]$ denotes the h_{th} head. Different colors correspond to various features. There are a total of 5 steps. (1) Input images to FEMs and obtain the support features X_s^h and query feature x_q^h . (2) Transform multi-head features to a unified space to obtain the novel features p_s^h, p_q^h . (3) Employ the transformed multi-head support features (e.g., p_s^h) to learn the combination weights Ω for each head, and assign them to the corresponding heads of features. (4) Collaboratively represent the samples by concatenating the weighted multi-head features. (5) Exploit the collaborative support features to construct classifier and recognize query sample.

\mathcal{D}_{novel} has totally different categories from \mathcal{D}_{base} . For more details, please refer to **Section 3**.

In the pre-train phase, researchers have designed a variety of classical FEMs for base samples. Each kind of model has a distinct emphasis. As examples, several may focus more attention on the contour information, whereas others may lay particular emphasis on the texture information. Thus, the description based on one category of features is often one-sided for samples, not sufficiently accurate. Besides, due to the negative influence of cross-domain (e.g., $\mathcal{D}_{base} \rightarrow \mathcal{D}_{novel}$, the trained FEM can not adapt to the novel class flawlessly), the novel data distribution may have a certain degree of deviation compared with the ground truth distribution. We dub this fundamental problem as a distribution-shift-problem (DSP).

Recent efforts on reducing the impact of DSP are generally based on designing a more robust and adaptive FEM to generate better features, such as introducing meta-learning strategy [10] [2]; self-supervised learning strategy [23] [30]; knowledge distillation strategy [38] [29]. Such methods merely weaken the influence of the DSP to a certain extent. This paper proposes to tackle the issue from a multi-modal learning perspective. We denote the multiple features extracted from different FEMs as multi-head features. Since the single-head feature is only one-sided for the sample, why do not attempt to conduct multi-head features fusion? We illustrate a t-SNE [41] visualization of different kinds of features in **Figure 1**.

However, two challenges prevent the idea. (1) Since the independent FEMs, the extracted multi-head features are in separate spaces, which exists a problem of inconsistent measurement scales. Thus, the first challenge is how to align the multi-head features. (2) Different features are suitable for various tasks. For example, features focusing on the contour information should be more crucial than features concentrating on texture information for classification

tasks. Therefore, the second challenge is how to weight multi-head features reasonably.

To tackle the DSP and overcome these two challenges, we propose a novel **Multi-Head Feature Collaboration (MHFC)** algorithm to improve the discrimination of sample’s feature. MHFC is a simple non-parametric model that can directly fuse multi-head features extracted from the existing FEMs, such as ICI-Net [47], MetaOpt-Net [2]. To solve the first challenge, we introduce a subspace learning method to transform the raw multi-head features to a unified space with reconstructed low-dimensional representation. It is also helpful to reduce redundant information. Next, we design an attention block to automatically update combination weights for each head of the feature to solve the second challenge efficiently. Finally, we generate the collaborative representation of the sample by concatenating the processed multi-head features. We illustrate the flowchart in **Figure 2**.

Besides, according to the data adopted in the design of the classifier, researchers categorize the FSL-based approaches as three sorts: (1) Inductive few-shot learning (IFSL). (2) Transductive few-shot learning (TFSL). (3) Semi-supervised few-shot learning (SSFSL). This paper extends the proposed MHFC to these three settings.

In summary, the main contributions focus on:

(1) We propose a novel method for FSL, dubbed as **Multi-Head Feature Collaboration (MHFC)** and extend it to three FSL-based settings. It addresses the DSP by comprehensively considering the multi-head features to improve the discrimination of sample’s representation.

(2) Compared to tuning the network to solve DSP, the proposed MHFC is more straightforward and effective. It is a simple non-parametric method that directly fuses multi-head features extracted from the existing FEMs. Besides, the more robust feature representation enables the proposed MHFC to achieve amazing performance especially when the samples are extremely scarce (e.g., inductive

setting on 5-way 1-shot case, please refer to **Table 1, 2**). Thus, we consider this paper may be meaningful to be applied in reality.

(3) We evaluate the proposed method on four benchmark datasets (mini-ImageNet, tiered-ImageNet, CIFAR-FS, FC100) and achieve significant improvements of **2.1%-7.8%** compared with other state-of-the-art methods. Besides, to prove that the proposed method can overcome DSP, we design the cross-domain experiments (e.g., mini-ImageNet \rightarrow CUB) and achieve far better performance than state-of-the-art methods of at least **7.8%**.

2 RELATED WORK

2.1 Few-Shot Learning

In the past decade, FSL based works have attracted lots of attention. Researchers have proposed various classical frameworks to solve this problem. We list the two most popular types, including (1) Meta-learning based methods, such as MAML [10], Reptile [24], LEO [34], which purpose to obtain a universal model to rapidly adapt to new tasks. (2) Metric learning based methods, focusing on looking for ideal distance metrics to strengthen model’s robustness, including ProtoNet [36], MetaOpt [2], TADAM [25] *et al.* In addition, all these methods can be split into another taxonomy, e.g. inductive few-shot learning (IFSL), transductive few-shot learning (TFSL), and semi-supervised few-shot learning (SSFSL). For example, MAML [10], LEO [34], S2M2 [23] *et al.* are based on inductive setting; DPGN [51], TEAM [27], SIB [12] *et al.* are TFSL methods; and LST [16], EPNet [30], ICI [47] *et al.* are based on semi-supervised setting.

2.2 Multi-Modal Learning

Just as every coin has two sides, it would be incomplete to define objects from a single perspective. Therefore, multi-modal learning has received wide attention in recent years. There exist lots of classical methods and corresponding applications. For example, Liu *et al.* proposed a sparse coding based multi-modal method MHDSC [21] for image annotation task; Liu *et al.* proposed SPM-CRC [19], which improves the collaborative representation model from multi-modal learning to classify remote sensing images; Jan *et al.* proposed MVCCA [32] and employed it in natural language processing. Liu *et al.* proposed MHL [20] to solve Alzheimer’s Disease Predicting problem; Zhang *et al.* proposed IMHL [55], which is an inductive hypergraph learning from multi-modal and applied it for 3D object recognition. All these methods may help FSL, and some multi-model based FSL methods were proposed, including [6] (introduced ensemble strategy in pretrain), [54] (adopted multi-head classifier in fine-tuning), [7] (fused multi-domain representation). This paper makes an orthogonal contribution towards efficient semantic-preserving pretraining.

2.3 Subspace Learning

Subspace learning is capable of transferring the samples to another representation. It is an efficient dimension reduction method. Here, we list several classical subspace learning methods, which have been employed in the proposed MHFC. The first one is Principal Component Analysis (PCA) [39]. It projects the raw features to a low-dimensional space by using singular value decomposition. The second one is Locally Linear Embedding (LLE) [31], which

tries to preserve distances within local according to seeking a low-dimensional projection of the data. The last one is Laplacian Eigenmap (LE) [1]. It exploits a spectral decomposition of the graph Laplacian to project the raw data to a low-dimensional representation. All these methods are helpful for our MHFC, and we will show the comparison results in **Section 4.2.1**.

3 PROBLEM FORMULATION

In this section, we introduce the complete procedure in details. It is composed of two phases, including pre-train and meta-test. i) In pre-train phase, given base data $\mathcal{D}_{base} = \{(x_i, y_i) | y_i \in C_{base}\}_{i=1}^{N_{base}}$, where x and y denote the sample and corresponding label, respectively. N_{base} denotes the total number of base data. C_{base} indicates the base category set. We train the CNN-based FEM $\mathcal{M}_\theta(\cdot)$ on \mathcal{D}_{base} , where θ indicates the parameters in CNN. In this paper, divers FEMs are employed to extract features for different heads, and we define the FEM on the h_{th} head as $\mathcal{M}_\theta^h(\cdot)$, where $h = 1, 2, \dots, H$, more details please refer to **Section 4.4**.

ii) For the meta-test phase, the novel data $\mathcal{D}_{novel} = \{(x_j, y_j) | y_j \in C_{novel}\}_{j=1}^{N_{novel}}$, where C_{novel} denotes the novel category set, N_{novel} denotes the number of novel data. $C_{base} \cap C_{novel} = \emptyset$. \mathcal{D}_{novel} includes three components, e.g., $\mathcal{D}_{novel} = \{\mathcal{S}, \mathcal{U}, \mathcal{Q}\}$, where \mathcal{S} , \mathcal{U} and \mathcal{Q} denote support set, unlabeled set and query set, $\mathcal{S} \cap \mathcal{U} = \emptyset$, $\mathcal{S} \cap \mathcal{Q} = \emptyset$, $\mathcal{Q} \cap \mathcal{U} = \emptyset$. In this phase, we first utilize the trained FEM to extract \mathcal{D}_{novel} ’s feature, then design a classifier to classify \mathcal{Q} . There exist three settings to design the classifier, e.g., inductive setting, transductive setting, and semi-supervised setting. **Section 4.3** show more details. We follow standard *C-way-T-shot* per episode as [47] for classification, where *C-way* denotes *C* classes, and *T-shot* indicates *T* samples per class. We average the accuracies of all the episodes with 95% confidence intervals as the final result.

4 METHODOLOGY

In this section, we first briefly review the linear regression classifier as an example to introduce our method. Then, we propose the novel **Multi-Head Feature Collaboration (MHFC)** algorithm to collaboratively represent the samples with processed multi-head features. Next, we extend the proposed MHFC to three kinds of few-shot learning settings. Finally, we introduce the employed multi-head feature extraction model.

4.1 Review of Linear Regression Classifier

This proposed method pays attention to the various features that can integrate all types of conventional classification strategy (such as linear regression, support vector machine, logistic regression). In this paper, we employ a simple regularized linear regression model as an example to show the details of our method. We formulate the objective function as:

$$\arg \min_{\mathbf{W}} \mathcal{F} = \|\mathbf{Y} - \mathbf{W}\mathbf{X}\|_F^2 + \mu \|\mathbf{W}\|_F^2 \quad (1)$$

where $\|\cdot\|_F$ represents (\cdot) ’s Frobenius-norm. μ is the hyperparameter. $\mathbf{X} = [\mathbf{x}_1, \mathbf{x}_2, \dots, \mathbf{x}_N] \in \text{https} : // \text{www.Overleaf.com/}$, $\mathbf{Y} = [\mathbf{y}_1, \mathbf{y}_2, \dots, \mathbf{y}_N] \in \mathbb{R}^{C \times N}$, $\dim 1$ and N indicate the dimension and number of labeled samples, respectively. C denotes the number of categories. $\mathbf{x}_n, \mathbf{y}_n$ ($n = 1, 2, \dots, N$) denote the feature embedding

vector and one-hot label vector of the n_{th} sample. $W \in \mathbb{R}^{C \times dim1}$ represents the to-be-learned classifier. We directly optimize the objective function and obtain the W as:

$$W = YX^T (XX^T + \mu I)^{-1} \quad (2)$$

where I is the identity matrix. Following, given a testing sample embedding $x_{ts} \in \mathbb{R}^{dim1}$, we predict the x_{ts} 's category by:

$$\mathcal{A}(x_{ts}) = \max \{Wx_{ts}\} \quad (3)$$

where \max denotes an operator to obtain the index of the max value in the vector.

4.2 Multi-Head Feature Collaboration

4.2.1 Multi-Head Feature Transformation. Since one kind of incomplete feature cannot reflect a sample well, we introduce various features to represent samples from different heads collaboratively. Assume that we have H heads in total. Each head corresponds to one kind of feature X^h , where $h = 1, 2, \dots, H$. As mentioned in **Section 1**, the multi-head features are in separate spaces, which exists a problem of inconsistent measurement scales.

To address this challenge, we introduce a conventional subspace learning method (denoted as $\mathcal{J}(\cdot)$) to transform the raw features into a unified space with reconstructed low-dimensional representation. Specifically, we treat H heads of the same sample as H samples, and denote the features of the expanded dataset as $X_{exp} = [X^1, X^2, \dots, X^H] \in \mathbb{R}^{dim1 \times (N \times H)}$. We conduct subspace learning operation $\mathcal{J}(X_{exp})$ and obtain the novel features $X'_{exp} = [P^1, P^2, \dots, P^H] \in \mathbb{R}^{dim2 \times (N \times H)}$, where $P^h \in \mathbb{R}^{dim2 \times N}$ denotes the feature on the h_{th} head after subspace transformation. $dim2$ denotes the novel dimension.

4.2.2 Multi-Head Feature Attention Block. Consider that the significance of these features is different per episode. We try to find the optimal combination weights $\Omega = [\Omega^1, \Omega^2, \dots, \Omega^H]^T$ to let these features have different influences for the final decision, where Ω is a weight vector, $\Omega^h (h = 1, 2, \dots, H)$ denotes the h_{th} element in Ω . We first employ the transformed feature P^h to replace X^h and obtain a novel classifier $W_p^h \in \mathbb{R}^{C \times dim2}$ according to **Equation 2**, where W_p^h indicates the trained novel classifier on the h_{th} head, which can be formulated as:

$$W_p^h = Y P^{hT} (P^h P^{hT} + \mu I)^{-1} \quad (4)$$

Then use P^h and W_p^h to re-calculate the objective function's loss on the h_{th} head \mathcal{F}_p^h by **Equation 1**, which can be formulated as:

$$\mathcal{F}_p^h = \|Y - W_p^h P^h\|_F^2 + \mu \|W_p^h\|_F^2 \quad (5)$$

Next, exploit the \mathcal{F}_p^h to compute the combination weights. The objective function can be formulated as:

$$\begin{aligned} \arg \min_{\Omega} &= \sum_{h=1}^H \left(\Omega^h \mathcal{F}_p^h \right) + \eta \|\Omega\|_2^2 \\ \text{s.t.} & \sum_{h=1}^H \Omega^h = 1 \quad \Omega^h \geq 0 \end{aligned} \quad (6)$$

where Ω^h indicates the weight of h_{th} head. $\|\cdot\|_2$ represents (\cdot) 's ℓ_2 -norm. η is the parameter. We introduce the Lagrangian to solve the problem, the **Equation 6** can be rewritten as:

$$\arg \min_{\Omega, \zeta, \Lambda} \mathcal{G} = \sum_{h=1}^H \left(\Omega^h \mathcal{F}_p^h \right) + \eta \|\Omega\|_2^2 - \zeta \left(\sum_{h=1}^H \Omega^h - 1 \right) - \Lambda^T \Omega \quad (7)$$

where ζ is a constant, $\Lambda = [\Lambda^1, \Lambda^2, \dots, \Lambda^H]^T$ is a vector. Assume $\hat{\Omega}, \hat{\zeta}, \hat{\Lambda}$ are the optimal solutions, we solved this problem as:

$$\hat{\Omega}^h = \frac{1}{2\eta} \max \left\{ \frac{\sum_{h=1}^H \mathcal{F}_p^h}{H} + \frac{2\eta}{H} - \mathcal{F}_p^h - \hat{\Lambda}_{avg}, 0 \right\} \quad (8)$$

where $\hat{\Lambda}_{avg}$ is a constant, denotes the average of $\hat{\Lambda}$. For the detailed optimization process, please refer to **Appendix A.2**.

4.2.3 Multi-Head Feature Collaborative Classifier. After giving multi-head features the combination weights, we obtain the final collaborative feature $Z = [z_1, z_2, \dots, z_N] \in \mathbb{R}^{dim3 \times N}$ by:

$$Z \leftarrow z_n = \text{Concat} \left(\hat{\Omega}^1 p_n^1, \hat{\Omega}^2 p_n^2, \dots, \hat{\Omega}^H p_n^H \right) \quad (9)$$

where $p_n^h, z_n^h (n = 1, 2, \dots, N)$ denote the n_{th} vector of P^h and Z^h .

Next, according to **Equation 2**, we use Z to replace X and obtain the final collaborative classifier $W_z \in \mathbb{R}^{C \times dim3}$, which can be formulated as:

$$W_z = Y Z^T (Z Z^T + \mu I)^{-1} \quad (10)$$

Finally, given a testing sample feature $x_{ts}^h (h = 1, 2, \dots, H)$, we first obtain the collaborative feature $z_{ts} \in \mathbb{R}^{dim3}$ by **Equation 8, 9**, then predict the label by:

$$\mathcal{A}(z_{ts}) = \max \{W_z z_{ts}\} \quad (11)$$

4.3 MHFC for Few-Shot Learning

Define the feature of \mathcal{D}_{novel} on the h_{th} head as $X_{novel}^h = [X_s^h, X_u^h, X_q^h]$, where $X_s^h = \mathcal{M}_{\theta}^h(\mathcal{S})$, $X_u^h = \mathcal{M}_{\theta}^h(\mathcal{U})$, and $X_q^h = \mathcal{M}_{\theta}^h(\mathcal{Q})$ denote the features of support, unlabeled, and query data on the h_{th} head. Thus, the (X_{novel}^h) 's feature after transformation can be defined as $P_{novel}^h = [P_s^h, P_u^h, P_q^h]$. Researchers employ different data to design the classifier, and these methods can be split into three settings, e.g., inductive setting, semi-supervised setting, and transductive setting.

4.3.1 Semi-Supervised MHFC. Semi-supervised setting in few-shot learning adopts the support set \mathcal{S} and unlabeled set \mathcal{U} to train the classifier, and then predict the query label. In this paper, we extend our MHFC to the semi-supervised setting by introducing a simple self-training strategy. It can employ the unlabeled data to strengthen the classifier. We show the detailed steps as:

(1) Exploit the support data to train the basic classifier on each head, **Equation 4** can be rewritten as:

$$W_p^h = Y_s P_s^{hT} (P_s^h P_s^{hT} + \mu I)^{-1} \quad (12)$$

where Y_s denotes the one-hot label matrix of support data.

(2) Calculate the combination weight on each head by:

$$\begin{cases} \mathcal{F}_p^h = \|Y_s - W_p^h P_s^h\|_F^2 + \mu \|W_p^h\|_F^2 \\ \hat{\Omega}^h = \frac{1}{2\eta} \max \left\{ \frac{\sum_{h=1}^H \mathcal{F}_p^h}{H} + \frac{2\eta}{H} - \mathcal{F}_p^h - \hat{\Lambda}_{avg}, 0 \right\} \end{cases} \quad (13)$$

(3) Obtain the collaborative feature of support set and classifier by:

$$\begin{cases} Z_s \leftarrow z_{sn} = \text{Concat} \left(\hat{\Omega}^1 p_{sn}^1, \hat{\Omega}^2 p_{sn}^2, \dots, \hat{\Omega}^H p_{sn}^H \right) \\ W_z = Y_s Z_s^T \left(Z_s Z_s^T + \mu I \right)^{-1} \end{cases} \quad (14)$$

where $p_{sn}^h (n = 1, 2, \dots, N)$ indicates the n_{th} vector in P_s^h . Z_s represents the collaborative feature of support set. z_{sn} denotes the n_{th} vector in Z_s .

(4) Utilize the trained classifier W_z to predict the unlabeled data \mathcal{U} by:

$$\begin{cases} Z_u \leftarrow z_{un} = \text{Concat} \left(\hat{\Omega}^1 p_{un}^1, \hat{\Omega}^2 p_{un}^2, \dots, \hat{\Omega}^H p_{un}^H \right) \\ Y_{pseudo} = W_z Z_u \end{cases} \quad (15)$$

where $p_{un}^h (n = 1, 2, \dots, N)$ indicates the n_{th} vectors in P_u^h . Z_u represents the collaborative feature embedding of the unlabeled set. z_{un} denotes the n_{th} vector in Z_u . Y_{pseudo} represents the predicted soft-pseudo-label of unlabeled data.

(5) Select one most confidence sample through the Y_{pseudo} without putting back, the corresponding one-hot-pseudo-label and feature (after transformation) are defined as y_{select} and p_{select}^h . Then, expand it to the support set by:

$$\begin{cases} P_s^h = \begin{bmatrix} p_s^h & p_{select}^h \end{bmatrix} \\ Y_s = \begin{bmatrix} Y_s & y_{select} \end{bmatrix} \end{cases} \quad (16)$$

(6) Repeat (1), (2) (3), (4), (5) until the performance of classifier is stable.

(7) Obtain the collaborative feature embedding of query data by:

$$Z_q \leftarrow z_{qn} = \text{Concat} \left(\hat{\Omega}^1 p_{qn}^1, \hat{\Omega}^2 p_{qn}^2, \dots, \hat{\Omega}^H p_{qn}^H \right) \quad (17)$$

where $p_{qn}^h (n = 1, 2, \dots, N)$ indicates the n_{th} vector in P_q^h . Z_q represents the collaborative feature of query data. z_{qn} denotes the n_{th} vector in Z_q .

(8) Finally, employ the optimal classifier to predict the query label by:

$$\mathcal{A}(Z_q) = \max \{W_z Z_q\} \quad (18)$$

We summarize the Algorithm in **Appendix A.1**.

4.3.2 Inductive MHFC. Unlike semi-supervised few-shot learning (SSFSL), inductive few-shot learning (IFSL) based methods only employ the support data to train the classifier and predict the query's category. IFSL can be viewed as the special case of SSFSL (e.g., there not exist unlabeled data). Thus, we can use the steps (e.g., (1), (2), (3), (7), (8)) to implement the inductive MHFC.

4.3.3 Transductive MHFC. In transductive few-shot learning (TFSL), besides the support data's features and label information, researchers also apply the features of query data to construct the classifier and then predict the query label. To implement the transductive MHFC, we need to make some adjustments to the step (4) in **Section 4.3.1**. We re-represent (4) as:

(9) Utilize the trained classifier W_z to predict the query data Q by:

$$\begin{cases} Z_q \leftarrow z_{qn} = \text{Concat} \left(\hat{\Omega}^1 p_{qn}^1, \hat{\Omega}^2 p_{qn}^2, \dots, \hat{\Omega}^H p_{qn}^H \right) \\ Y_{pseudo} = W_z Z_q \end{cases} \quad (19)$$

where $p_{qn}^h (n = 1, 2, \dots, N)$ indicates the n_{th} vectors in P_q^h . Z_q represents the collaborative feature embedding of the unlabeled set. z_{qn} denotes the n_{th} vector in Z_q . Y_{pseudo} represents the predicted soft-pseudo-label of query data.

After that, we achieve transductive MHFC by steps (1), (2), (3), (9), (5), (6), (8).

4.4 Multi-Head Feature Extraction Model

The multi-head features we adopted come from different feature extraction models (FEMs). As examples: (1) Standard feature (Std-Fea), the FEM utilizes a standard CNN-based classification structure, such as [47]. (2) Meta feature (Meta-Fea), the FEM introduces the meta-learning strategy to the network, just like [2]. (3) Self-supervised-feature (SS-Fea), the FEM adds auxiliary losses to the standard CNN-based classification structure from a self-supervised perspective to strengthen the robustness of the network, similar as [23]. We discuss the results of all kinds of stacking ways in **Appendix B.2**.

In this paper, we merely fuse two kinds of SS-Feas for most of the experiments as an example for convenience. For the first category, we design the FEM by introducing standard classification loss \mathcal{L}_c and auxiliary rotation loss \mathcal{L}_r . \mathcal{L}_c can be formulated as:

$$\mathcal{L}_c = - \sum_c y_{(c,x)} \log(p_{(c,x)}) \quad (20)$$

where $c \in C_{base}$ denotes the c_{th} class. $y_{(c,x)}$, $p_{(c,x)}$ indicate the probabilities that the truth label and predicted label of x_{th} sample belongs to c_{th} class. Then, we rotate each sample to r degree and $r \in C_R = \{0^\circ, 90^\circ, 180^\circ, 270^\circ\}$. We define rotation loss as:

$$\mathcal{L}_r = - \sum_r y_{(r,x)} \log(p_{(r,x)}) \quad (21)$$

where $y_{(r,x)}$, $p_{(r,x)}$ indicate the probabilities that the truth label and predicted label of x_{th} sample belongs to r_{th} class. Thus, the first loss function is defined as $\mathcal{L}_c + \mathcal{L}_r$, and the feature based on this kind of FEM is dubbed as SS-R-Fea.

The second feature is denoted as SS-M-Fea, which extracted from another category of self-supervised FEM. Specifically, this FEM adds the loss \mathcal{L}_c and auxiliary mirror loss \mathcal{L}_m to the neural network to predict image mirrors. Assume that there are m ways and $m \in C_M = \{vertically, horizontally, diagonally\}$, we define the mirror loss as:

$$\mathcal{L}_m = - \sum_m y_{(m,x)} \log(p_{(m,x)}) \quad (22)$$

where $y_{(m,x)}$, $p_{(m,x)}$ indicate the probabilities that the truth label and predicted label of x_{th} sample belongs to m_{th} class. Next, we summarize the loss function as $\mathcal{L}_c + \mathcal{L}_m$.

5 EXPERIMENTS

In this section, we first briefly review the benchmark datasets and show the implementation details. Then, we list the experimental results in **Table 1, 2** and analyse them. Next, we perform ablation studies to discuss the factors that influence MHFC’s performance, e.g., multi-head feature fusion, subspace transformation, and attention block that calculates the combination weights. In the following, we take a cross-domain experiment to further evaluate the ability and robustness of the proposed method. We conduct all the experiments on a Tesla-V100 GPU with 32G memory. All the source codes will be made available to the public.

5.1 Datasets

We carry out experiments on five benchmark datasets, including mini-ImageNet [43], tiered-ImageNet [28], CIFAR-FS [2], FC100 [25], and CUB [44]. Both **mini-ImageNet** and **tiered-ImageNet** are the subsets of ImageNet dataset [33]. mini-ImageNet consists of 100 classes and tiered-ImageNet contains 608 classes. For both datasets, the number of images for each class is 600 and the size of each image is 84×84 . We follow standard split as [47], selecting 64 classes as the base set, 16 classes as the validation set, 20 classes as the novel set for mini-ImageNet, and selecting 351 classes as the base set, 97 classes as the validation set, 160 classes as the novel set for tiered-ImageNet. Both **CIFAR-FS** and **FC100** are the subsets of CIFAR-100 dataset [14], and consist of 100 classes. We follow the split introduced in [2] to divide CIFAR-FS into 64 classes as base set, 16 classes as validation set, 20 classes as novel set, and divide FC100 into 60 classes as base set, 20 classes as validation set, 20 classes as novel set. All the image size is 32×32 . **CUB** totally includes 11,788 images with 200 categories. We follow the setting in ICI [47] to split it into 100 classes as base set, 50 classes as validation set and 50 classes as novel set. The images are cropped into 84×84 .

5.2 Implementation Details

In this paper, all the FEMs on different heads adopt the ResNet12 [11] backbone, consisting of four residual blocks (3×3 convolution layer, batch normalization layer, LeakyReLU layer), four 2×2 max pooling layers, and four dropout layers. We adopt stochastic gradient descent (SGD) optimizer with Nesterov momentum (0.9) for the optimizer. For the parameter η in **Equation 6**, we fix it to 1.4 for convenience. We set the training epochs to 120 and test over 600 episodes with 15 query samples per class for all the models. Besides, the selected subspace learning methods all follow the default implementation of scikit-learn [26]. And there has no fine-tuning process when classifying the novel data. For other settings, such as the learning rate, data augmentation, filters’ number, we follow the ICI [47].

5.3 Experimental Results

We compare the proposed MHFC (only fuse SS-F-Fea and SS-M-Fea) with several state-of-the-art methods, the results are listed in **Table 1 and 2**. Here, we list several observations.

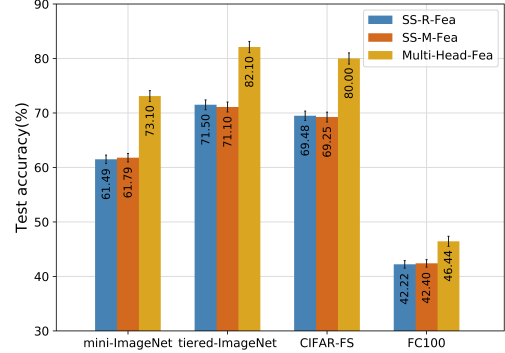


Figure 3: Ablation studies to show the performances of employing different kinds of features with the inductive setting.

(1) Researchers split the few-shot learning methods into three settings, e.g., inductive, transductive, and semi-supervised. While, in the related works of FSL, the results on all settings are usually compared together. Compared with the methods proposed recently, our MHFC has achieved state-of-the-art performance. It has far surpassed other models on the four datasets, especially on 5-way 1-shot case, the MHFC outperforms other methods at least **4.4%**, **2.1%**, **7.7%** and **7.8%** on mini-ImageNet, tiered-ImageNet, CIFAR-FS, FC100 datasets. Our results on the 5-way 1-shot case are even better than many other methods on the 5-way 5-shot case. And on the 5-way 5-shot case, the MHFC also exceeds others at least **3.0%**, **2.8%**, **4.8%** and **6.9%** on mini-ImageNet, tiered-ImageNet, CIFAR-FS, FC100 datasets.

(2) Compared with the methods of each setting, our proposed MHFC has achieved excellent performances, in particular on the 5-way 1-shot case with the inductive setting. MHFC has significant improvements of at least **7.7%**, **10.0%**, **6.8%** and **4.7%** on mini-ImageNet, tiered-ImageNet, CIFAR-FS, FC100 datasets. Notably, the performance of MHCF with the inductive setting has exceeded many other methods with transductive or semi-supervised settings. Besides, for the methods based on semi-supervised setting, the final results are influenced by the number of employed unlabeled samples. Thus, we observe the impact and list the results in **Appendix B.1**. With the increase of unlabeled samples, the proposed method has become more effective. And the results start to saturate after 100 unlabeled samples.

5.4 Ablation Studies

In this paper, we propose MHFC for few-shot learning. There exist three factors influence the classification performance, e.g., (1) introducing multi-head features; (2) transforming the multi-head features into a unified space; (3) designing attention mechanism to weight features. This section conducts ablation studies on 5-way 1-shot case with the inductive setting to evaluate the efficiency of the three blocks.

Table 1: The 5-way few-shot classification accuracies on mini-ImageNet and tiered-ImageNet with 95% confidence intervals over 600 episodes. $(\cdot)^*$, $(\cdot)^\dagger$, and $(\cdot)^\ddagger$ in Table 1, 2, 4 indicate inductive, transductive, and semi-supervised settings, respectively. 4CONV, ResNet12, ResNet18 and WRN are the exploited FEM’s architectures. The (80), (100) in the semi-supervised setting indicate the number of employed unlabeled samples per class. The top two results are shown in red and blue, respectively.

Method	Backbone	mini-ImageNet		tiered-ImageNet	
		5-way 1-shot	5-way 5-shot	5-way 1-shot	5-way 5-shot
Baseline [*] [4] (ICLR,2019)	ResNet18	51.75 \pm 0.80	74.27 \pm 0.63	-	-
Baseline++ [*] [4] (ICLR,2019)	ResNet18	51.87 \pm 0.77	75.68 \pm 0.63	-	-
TapNet [*] [52] (ICML,2019)	ResNet12	61.65 \pm 0.15	76.36 \pm 0.10	63.08 \pm 0.15	80.26 \pm 0.12
LEO [*] [34] (ICLR,2019)	WRN	61.76 \pm 0.08	77.59 \pm 0.12	66.33 \pm 0.05	81.44 \pm 0.09
AM3 [*] [48] (NIPS,2019)	ResNet12	65.30 \pm 0.49	78.10 \pm 0.36	69.08 \pm 0.47	82.58 \pm 0.31
CTM [*] [15] (CVPR,2019)	ResNet18	64.12 \pm 0.82	80.51 \pm 0.13	-	-
MABAS [*] [13] (ECCV,2020)	ResNet12	64.21 \pm 0.82	81.01 \pm 0.57	-	-
MELR [*] [9] (ICLR,2021)	ResNet12	67.40 \pm 0.43	83.40 \pm 0.28	72.14 \pm 0.51	87.01 \pm 0.35
Our MHFC[*]	ResNet12	73.10 \pm 1.00	81.75 \pm 0.56	82.10 \pm 1.03	87.99 \pm 0.60
TPN [†] [22] (ICLR,2019)	4CONV	55.51 \pm 0.86	69.86 \pm 0.65	59.91 \pm 0.94	73.30 \pm 0.75
TEAM [†] [27] (ICCV,2019)	ResNet12	60.07 \pm 0.63	75.90 \pm 0.52	-	-
Fine-tuning [†] [5] (ICLR,2020)	WRN	65.73 \pm 0.68	78.40 \pm 0.52	73.34 \pm 0.71	85.50 \pm 0.50
DPGN [†] [51] (CVPR,2020)	ResNet12	67.77 \pm 0.32	84.60 \pm 0.43	72.45 \pm 0.51	87.24 \pm 0.39
ODE [†] [49] (CVPR,2021)	ResNet12	67.76 \pm 0.46	82.71 \pm 0.31	71.89 \pm 0.52	85.96 \pm 0.35
Our MHFC[†]	ResNet12	74.81 \pm 1.12	85.58 \pm 0.61	83.95 \pm 1.13	90.75 \pm 0.58
TPN [‡] [22] (ICLR,2019)	4CONV	52.78 \pm 0.27	66.42 \pm 0.21	55.74 \pm 0.29	71.01 \pm 0.23
LST [‡] (100) [16] (NIPS,2019)	ResNet12	70.10 \pm 1.90	78.70 \pm 0.80	77.70 \pm 1.60	85.20 \pm 0.80
EPNet [‡] (100) [30] (ECCV,2020)	ResNet12	75.36 \pm 1.01	84.07 \pm 0.60	81.79 \pm 0.97	88.45 \pm 0.61
TransMatch [‡] (100) [53] (CVPR,2020)	WRN	63.02 \pm 1.07	81.19 \pm 0.59	-	-
ICI [‡] (80) [47] (CVPR,2020)	ResNet12	71.41	81.12	85.44	89.12
Our MHFC[‡] (80)	ResNet12	79.26 \pm 1.14	87.30 \pm 0.55	87.57 \pm 1.03	91.80 \pm 0.56
Our MHFC[‡] (100)	ResNet12	79.76 \pm 1.16	87.64 \pm 0.53	87.56 \pm 1.04	91.90 \pm 0.56

Table 2: The 5-way few-shot classification accuracies on CIFAR-FS and FC100 with 95% confidence intervals over 600 episodes. The top two results are shown in red and blue, respectively.

Method	Backbone	CIFAR-FS		FC100	
		5-way 1-shot	5-way 5-shot	5-way 1-shot	5-way 5-shot
ProtoNet [*] [36] (NIPS,2017)	4CONV	55.50 \pm 0.70	72.00 \pm 0.60	35.30 \pm 0.60	48.60 \pm 0.60
MAML [*] [10] (ICML,2018)	4CONV	58.90 \pm 1.90	71.50 \pm 1.00	-	-
MABAS [*] [13] (ECCV,2020)	ResNet12	73.24 \pm 0.95	85.65 \pm 0.65	41.74 \pm 0.73	57.11 \pm 0.75
Our MHFC[*]	ResNet12	80.00 \pm 1.02	86.33 \pm 0.61	46.44 \pm 0.93	59.41 \pm 0.72
TEAM [†] [27] (ICCV,2019)	ResNet12	70.43 \pm 1.03	81.25 \pm 0.92	-	-
Fine-tuning [†] [5] (ICLR,2020)	WRN	76.58 \pm 0.68	85.79 \pm 0.50	43.16 \pm 0.59	57.57 \pm 0.55
Our MHFC[†]	ResNet12	81.83 \pm 1.16	89.27 \pm 0.63	47.02 \pm 1.05	61.88 \pm 0.80
ICI [‡] (80) [47] (CVPR,2020)	ResNet12	78.07	84.76	-	-
Our MHFC[‡] (80)	ResNet12	84.74 \pm 1.14	90.19 \pm 0.63	50.95 \pm 1.11	64.05 \pm 0.82
Our MHFC[‡] (100)	ResNet12	85.76 \pm 1.08	90.42 \pm 0.64	50.72 \pm 1.09	64.45 \pm 0.83

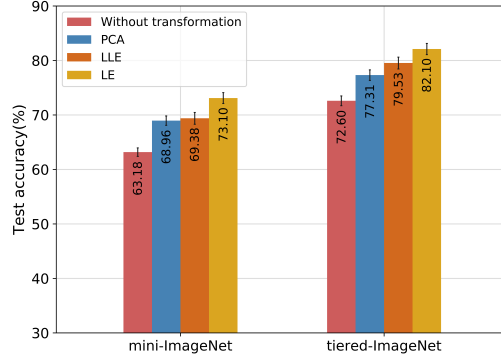


Figure 4: The comparison results of adding transformation or not on 5-way 1-shot case with the inductive setting.

Table 3: Comparison results with fixed weights on 5-way few-shot case. (a, b) denotes that the SS-R-Fea’s weight is "a", and SS-M-Fea’s weight is "b". MHFC employs our designed attention block to update the weights automatically for each episode. The top two results are shown in red and blue.

Weight	mini-ImageNet		tiered-ImageNet	
	1-shot	5-shot	1-shot	5-shot
(0.1, 0.9)	70.85	80.09	79.66	87.12
(0.3, 0.7)	71.32	80.72	80.25	87.14
(0.5, 0.5)	71.88	80.15	80.86	87.38
(0.7, 0.3)	70.56	80.48	80.19	87.19
(0.9, 0.1)	70.36	79.97	79.69	86.93
MHFC	73.10	81.75	82.10	87.99

5.4.1 Influence of Multi-Head Feature. The results listed in Table 1, 2 employ two heads of features (SS-R-Fea and SS-M-Fea). Here, we compare the results of employing the raw single-head feature with the collaborative feature (e.g., multi-head-fea). The results of four datasets on 5-way 1-shot case with inductive setting are listed in Figure 3. Obviously, employing the collaborative feature improves significantly compared with exploiting the raw single-head feature. It demonstrates the efficiency of our "multi-head feature" to some extent. Moreover, the proposed model can integrate more than two heads of features. We list the comparison results in Appendix B.2.

5.4.2 Influence of Subspace Transformation. For all the results listed in Table 1, 2 with inductive setting, we select LE [1] to transform the multi-head features. While, besides the LE, there also exist several other choices to pull multi-head features to a unified space, such as PCA [39], LLE [31]. We illustrate Figure 4 to show the comparison results. We can see that all kinds of subspace learning methods are helpful to our MHFC, and LE is the most.

Table 4: Comparison in cross-domain dataset scenario. Our MHFC is in transductive setting. $(\cdot)^b$ and $(\cdot)^\#$ indicate the reported results come from [3] and [23], respectively. The top two results are shown in red and blue.

Method	mini-ImageNet \rightarrow CUB	
	5-way 1-shot	5-way 5-shot
Baseline ^b [4]	-	53.1
ProtoNet ^b [36]	-	62.0
RelationNet ^b [37]	-	57.7
GNN ^b [40]	-	66.9
Neg-Cosine ^b [18]	-	67.0
LaplacianShot ^b [56]	-	66.3
TIM-GD ^b [3]	-	71.0
MetaOpt [#] [2]	44.79 \pm 0.75	64.98 \pm 0.68
Manifold Mixup [#] [42]	46.21 \pm 0.77	66.03 \pm 0.71
S2M2 [#] [23]	48.24 \pm 0.84	70.44 \pm 0.75
MHFC [†]	61.57 \pm 1.28	78.80 \pm 0.78

5.4.3 Influence of Attention Block. We can use multi-head features to describe a category of samples, but the degrees of importance are different on each head. To this end, it is crucial to design the attention block to calculate weights for different categories automatically. Here, we compare the results with fixed weights to our MHFC, which is listed in Table 3. The results show that the updated weights are more reasonable for our method. Besides, from Equation 6, we know that η is a parameter to influence the to-be-learned weights. For fairness and convenience, we have fixed η to 1.4 for all the experiments. We list the other comparison results in Appendix B.3.

5.5 Cross-Domain Few-Shot Learning

After introducing multi-head features from different views, we believe that the MHFC is an extremely robust method in practical scenarios. Therefore, we evaluate the proposed method with transductive setting on a cross-domain dataset: e.g., mini-ImageNet \rightarrow CUB. In pre-train stage, we use mini-ImageNet to train the FEM, and in meta-test stage, we classify the CUB dataset. The results are reported in Table 4. Compared to the state-of-the-arts, we have significant improvements at least 13.3% on 1-shot case and 7.8% on 5-shot case. Thus, the performance on the cross-domain few-shot learning task demonstrates that the MHFC can solve the DSP better, and the proposed MHFC would be powerful in real practice.

6 CONCLUSION

Few-shot learning (FSL) based tasks have a fundamental problem, e.g., distribution-shift-problem (DSP). To address this challenge, we propose Multi-Head Feature Collaboration (MHFC), which attempts to collaboratively represent samples by fusing multi-head features. It is helpful to strengthen the FSL based model’s efficacy and robustness. MHFC is a simple non-parametric method that

can directly employ the existing FEMs. Experimental results have demonstrated the effectiveness of MHFC.

ACKNOWLEDGMENT

The paper was supported by the National Natural Science Foundation of China (Grant No. 62072468), the Natural Science Foundation of Shandong Province, China (Grant No. ZR2019MF073), the Fundamental Research Funds for the Central Universities, China University of Petroleum (East China) (Grant No. 20CX05001A), the Graduate Innovation Project of China University of Petroleum (East China) (YCX2021117, YCX2021123).

REFERENCES

- [1] Mikhail Belkin and Partha Niyogi. 2002. Laplacian eigenmaps and spectral techniques for embedding and clustering. In *NeurIPS*. 585–591.
- [2] Luca Bertinetto, Joao F. Henriques, Philip Torr, and Andrea Vedaldi. 2019. Meta-learning with differentiable closed-form solvers. In *ICLR*.
- [3] Malik Boudiaf, Ziko Imtiaz Masud, Jérôme Rony, José Dolz, Pablo Piantanida, and Ismail Ben Ayed. 2020. Transductive information maximization for few-shot learning. In *NeurIPS*.
- [4] Wei-Yu Chen, Yen-Cheng Liu, Zsolt Kira, Yu-Chiang Frank Wang, and Jia-Bin Huang. 2019. A closer look at few-shot classification. In *ICLR*.
- [5] Guneet S Dhillon, Pratik Chaudhari, Avinash Ravichandran, and Stefano Soatto. 2020. A baseline for few-shot image classification. In *ICLR*.
- [6] Nikita Dvornik, Cordelia Schmid, and Julien Mairal. 2019. Diversity with cooperation: Ensemble methods for few-shot classification. In *ICCV*. 3723–3731.
- [7] Nikita Dvornik, Cordelia Schmid, and Julien Mairal. 2020. Selecting relevant features from a multi-domain representation for few-shot classification. In *ECCV*. Springer, 769–786.
- [8] Baoyu Fan, Li Wang, Runze Zhang, Zhenhua Guo, Yaqian Zhao, Rengang Li, and Weifeng Gong. 2020. Contextual Multi-Scale Feature Learning for Person Re-Identification. In *ACMMM*. 655–663.
- [9] Nanyi Fei, Zhiwu Lu, Tao Xiang, and Songfang Huang. 2021. Melr: Meta-learning via modeling episode-level relationships for few-shot learning. In *ICLR*.
- [10] Chelsea Finn, Pieter Abbeel, and Sergey Levine. 2017. Model-agnostic meta-learning for fast adaptation of deep networks. In *ICML*. 1126–1135.
- [11] Kaiming He, Xiangyu Zhang, Shaoqing Ren, and Jian Sun. 2016. Deep residual learning for image recognition. In *CVPR*. 770–778.
- [12] Shell Xu Hu, Pablo G Moreno, Yang Xiao, Xi Shen, Guillaume Obozinski, Neil D Lawrence, and Andreas Damianou. 2020. Empirical Bayes Transductive Meta-Learning with Synthetic Gradients. In *ICLR*.
- [13] Jaekyeom Kim, Hyoungseok Kim, and Gunhee Kim. 2020. Model-Agnostic Boundary-Adversarial Sampling for Test-Time Generalization in Few-Shot learning. *ECCV* (2020), 599–617.
- [14] Alex Krizhevsky, Geoffrey Hinton, et al. 2009. Learning multiple layers of features from tiny images. *Computer Science Department, University of Toronto* (2009).
- [15] Hongyang Li, David Eigen, Samuel Dodge, Matthew Zeiler, and Xiaogang Wang. 2019. Finding task-relevant features for few-shot learning by category traversal. In *CVPR*. 1–10.
- [16] Xinzhe Li, Qianru Sun, Yaoyao Liu, Qin Zhou, Shibao Zheng, Tat-Seng Chua, and Bernt Schiele. 2019. Learning to self-train for semi-supervised few-shot classification. In *NeurIPS*, Vol. 32. 10276–10286.
- [17] Shisong Lin, Mengchao Bai, Feng Liu, Linlin Shen, and Yicong Zhou. 2020. Orthogonalization-guided feature fusion network for multimodal 2D+ 3D facial expression recognition. *TMM* 23 (2020), 1581–1591.
- [18] Bin Liu, Yue Cao, Yutong Lin, Qi Li, Zheng Zhang, Mingsheng Long, and Han Hu. 2020. Negative margin matters: Understanding margin in few-shot classification. In *ECCV*. 438–455.
- [19] Bao-Di Liu, Jie Meng, Wen-Yang Xie, Shuai Shao, Ye Li, and Yanjiang Wang. 2019. Weighted spatial pyramid matching collaborative representation for remote-sensing-image scene classification. *Remote Sensing* 11, 5 (2019), 518.
- [20] Mingxia Liu, Yue Gao, Pew-Thian Yap, and Dinggang Shen. 2017. Multi-hypergraph learning for incomplete multimodality data. *IEEE Journal of Biomedical and Health Informatics* 22, 4 (2017), 1197–1208.
- [21] Weifeng Liu, Dacheng Tao, Jun Cheng, and Yuanyan Tang. 2014. Multiview Hessian discriminative sparse coding for image annotation. *Computer Vision and Image Understanding* 118 (2014), 50–60.
- [22] Yanbin Liu, Juho Lee, Minseop Park, Saehoon Kim, Eunho Yang, Sung Ju Hwang, and Yi Yang. 2019. Learning to propagate labels: Transductive propagation network for few-shot learning. In *ICLR*.
- [23] Puneet Mangla, Nupur Kumari, Abhishek Sinha, Mayank Singh, Balaji Krishnamurthy, and Vineeth N Balasubramanian. 2020. Charting the right manifold: Manifold mixup for few-shot learning. In *CVPR*. 2218–2227.
- [24] Alex Nichol, Joshua Achiam, and John Schulman. 2018. On first-order meta-learning algorithms. *arXiv preprint arXiv:1803.02999* (2018).
- [25] Boris Oreshkin, Pau Rodríguez López, and Alexandre Lacoste. 2018. Tadam: Task dependent adaptive metric for improved few-shot learning. In *NeurIPS*. 721–731.
- [26] Fabian Pedregosa, Gaël Varoquaux, Alexandre Gramfort, Vincent Michel, Bertrand Thirion, Olivier Grisel, Mathieu Blondel, Peter Prettenhofer, Ron Weiss, Vincent Dubourg, et al. 2011. Scikit-learn: Machine learning in Python. *Journal of Machine Learning Research* 12 (2011), 2825–2830.
- [27] Limeng Qiao, Yemin Shi, Jia Li, Yaowei Wang, Tiejun Huang, and Yonghong Tian. 2019. Transductive episodic-wise adaptive metric for few-shot learning. In *ICCV*. 3603–3612.
- [28] Mengye Ren, Eleni Triantafillou, Sachin Ravi, Jake Snell, Kevin Swersky, Joshua B Tenenbaum, Hugo Larochelle, and Richard S Zemel. 2018. Meta-learning for semi-supervised few-shot classification. In *ICLR*.
- [29] Mamshad Nayeem Rizve, Salman Khan, Fahad Shahbaz Khan, and Mubarak Shah. 2021. Exploring Complementary Strengths of Invariant and Equivariant Representations for Few-Shot Learning. In *CVPR*.
- [30] Pau Rodríguez, Issam Laradji, Alexandre Drouin, and Alexandre Lacoste. 2020. Embedding Propagation: Smoother Manifold for Few-Shot Classification. In *ECCV*. 121–138.
- [31] Sam T Roweis and Lawrence K Saul. 2000. Nonlinear dimensionality reduction by locally linear embedding. *Science* 290, 5500 (2000), 2323–2326.
- [32] Jan Ruppnik and John Shawe-Taylor. 2010. Multi-view canonical correlation analysis. In *KDD*. 1–4.
- [33] Olga Russakovsky, Jia Deng, Hao Su, Jonathan Krause, Sanjeev Satheesh, Sean Ma, Zhiheng Huang, Andrej Karpathy, Aditya Khosla, Michael Bernstein, et al. 2015. Imagenet large scale visual recognition challenge. *IJCV* 115, 3 (2015), 211–252.
- [34] Andrei A Rusu, Dushyant Rao, Jakub Sygnowski, Oriol Vinyals, Razvan Pascanu, Simon Osindero, and Raia Hadsell. 2019. Meta-learning with latent embedding optimization. In *ICLR*.
- [35] Shuai Shao, Rui Xu, Weifeng Liu, Bao-Di Liu, and Yan-Jiang Wang. 2020. Label embedded dictionary learning for image classification. *Neurocomputing* 385 (2020), 122–131.
- [36] Jake Snell, Kevin Swersky, and Richard Zemel. 2017. Prototypical networks for few-shot learning. In *NeurIPS*. 4077–4087.
- [37] Flood Sung, Yongxin Yang, Li Zhang, Tao Xiang, Philip HS Torr, and Timothy M Hospedales. 2018. Learning to compare: Relation network for few-shot learning. In *CVPR*. 1199–1208.
- [38] Yonglong Tian, Yue Wang, Dilip Krishnan, Joshua B Tenenbaum, and Phillip Isola. 2020. Rethinking few-shot image classification: a good embedding is all you need?. In *CVPR*.
- [39] Michael E Tipping and Christopher M Bishop. 1999. Probabilistic principal component analysis. *Journal of the Royal Statistical Society: Series B (Statistical Methodology)* 61, 3 (1999), 611–622.
- [40] Hung-Yu Tseng, Hsin-Ying Lee, Jia-Bin Huang, and Ming-Hsuan Yang. 2020. Cross-domain few-shot classification via learned feature-wise transformation. In *ICLR*.
- [41] Laurens Van der Maaten and Geoffrey Hinton. 2008. Visualizing data using t-SNE. *Journal of Machine Learning Research* 9, 11 (2008).
- [42] Vikas Verma, Alex Lamb, Christopher Beckham, Amir Najafi, Ioannis Mitliagkas, David Lopez-Paz, and Yoshua Bengio. 2019. Manifold mixup: Better representations by interpolating hidden states. In *ICML*. 6438–6447.
- [43] Oriol Vinyals, Charles Blundell, Timothy Lillicrap, Daan Wierstra, et al. 2016. Matching networks for one shot learning. In *NeurIPS*, Vol. 29. 3630–3638.
- [44] Catherine Wah, Steve Branson, Peter Welinder, Pietro Perona, and Serge Belongie. 2011. The caltech-ucsd birds-200-2011 dataset. (2011).
- [45] Dongkai Wang and Shiliang Zhang. 2020. Unsupervised person re-identification via multi-label classification. In *CVPR*. 10981–10990.
- [46] Li Wang, Baoyu Fan, Zhenhua Guo, Yaqian Zhao, Runze Zhang, Rengang Li, and Weifeng Gong. 2020. Dense-Scale Feature Learning in Person Re-Identification. In *ACCV*.
- [47] Yikai Wang, Chengming Xu, Chen Liu, Li Zhang, and Yanwei Fu. 2020. Instance credibility inference for few-shot learning. In *CVPR*. 12836–12845.
- [48] Chen Xing, Negar Rostamzadeh, Boris Oreshkin, and Pedro O Pinheiro. 2019. Adaptive cross-modal few-shot learning. In *NeurIPS*. 4847–4857.
- [49] Chengming Xu, Chen Liu, Li Zhang, Chengjie Wang, Jilin Li, Feiyue Huang, Xiangyang Xue, and Yanwei Fu. 2021. Learning Dynamic Alignment via Meta-filter for Few-shot Learning. In *CVPR*.
- [50] Yan Yan, Feiping Nie, Wen Li, Chenqiang Gao, Yi Yang, and Dong Xu. 2016. Image classification by cross-media active learning with privileged information. *TMM* 18, 12 (2016), 2494–2502.
- [51] Ling Yang, Liangliang Li, Zilun Zhang, Xinyu Zhou, Erjin Zhou, and Yu Liu. 2020. DPGN: Distribution Propagation Graph Network for Few-shot Learning. In *CVPR*. 13390–13399.
- [52] Sung Whan Yoon, Jun Seo, and Jaekyun Moon. 2019. Tapnet: Neural network augmented with task-adaptive projection for few-shot learning. In *ICML*. 7115–7123.

- [53] Zhongjie Yu, Lin Chen, Zhongwei Cheng, and Jiebo Luo. 2020. TransMatch: A Transfer-Learning Scheme for Semi-Supervised Few-Shot Learning. In *CVPR*. 12856–12864.
- [54] Zhongqi Yue, Hanwang Zhang, Qianru Sun, and Xian-Sheng Hua. 2020. Inter-ventional few-shot learning. In *NeurIPS*.
- [55] Zizhao Zhang, Haojie Lin, Xibin Zhao, Rongrong Ji, and Yue Gao. 2018. Inductive multi-hypergraph learning and its application on view-based 3D object classification. *TIP* 27, 12 (2018), 5957–5968.
- [56] Imtiaz Ziko, Jose Dolz, Eric Granger, and Ismail Ben Ayed. 2020. Laplacian regularized few-shot learning. In *ICML*. 11660–11670.

A METHODOLOGY

A.1 Algorithm

We have introduced our MHFC on semi-supervised setting in **Section 4.3.1**. Here, we show the details in **Algorithm 1**. **Eqa.** denotes the equation in the original paper.

Algorithm 1: Semi-Supervised MHFC

Input: Base set \mathcal{D}_{base} , Novel set $\mathcal{D}_{novel} = \{\mathcal{S}, \mathcal{U}, \mathcal{Q}\}$

Output: Query label

- 1 Design the multi-head feature extraction model $\mathcal{M}_\theta^h(\cdot)$ through \mathcal{D}_{base} , and obtain novel data' embedding by $X_s^h = \mathcal{M}_\theta^h(\mathcal{S})$, $X_u^h = \mathcal{M}_\theta^h(\mathcal{U})$, $X_q^h = \mathcal{M}_\theta^h(\mathcal{Q})$.
 - 2 Transform the novel data's embedding to an unified space and obtain P_s^h, P_u^h, P_q^h .
 - 3 **repeat**
 - 4 Train a basic classifier W_z by **Eqa. 12, 13, 14**.
 - 5 Predict the unlabeled data by **Eqa. 15**
 - 6 Select the most confidence sample and expand it to the support set by **Eqa. 16**.
 - 7 **until** the performance of to-be-learned classifier is stable.
 - 8 Concatenate multi-head query embedding by **Eqa. 17**.
 - 9 Utilize the optimal classifier to predict the query label by **Eqa. 18**.
-

A.2 Optimization of Combination Weights

The objective function to compute the combination weights $\Omega = [\Omega^1, \Omega^2, \dots, \Omega^H]^T$ can be formulated as:

$$\begin{aligned} \arg \min_{\Omega} \sum_{h=1}^H \left(\Omega^h \mathcal{F}_p^h \right) + \eta \|\Omega\|_2^2 \\ \text{s.t.} \quad \sum_{h=1}^H \Omega^h = 1 \quad \Omega^h \geq 0 \end{aligned} \quad (23)$$

where Ω is a weight vector, $\Omega^h (h = 1, 2, \dots, H)$ denotes the h_{th} element in Ω . \mathcal{F}_p^h indicates the loss of h_{th} head. We introduce the Lagrangian to solve the problem, the **Equation 23** is rewritten as:

$$\arg \min_{\Omega, \zeta, \Lambda} \mathcal{G} = \sum_{h=1}^H \left(\Omega^h \mathcal{F}_p^h \right) + \eta \|\Omega\|_2^2 - \zeta \left(\sum_{h=1}^H \Omega^h - 1 \right) - \Lambda^T \Omega \quad (24)$$

where ζ is a constant, $\Lambda = [\Lambda^1, \Lambda^2, \dots, \Lambda^H]^T$ is a vector. For convenience, we rewrite this equation into a matrix form as:

$$\arg \min_{\Omega, \zeta, \Lambda} \mathcal{G} = \Omega^T \mathbf{F} + \eta \|\Omega\|_2^2 - \zeta \left(\Omega^T \mathbf{1} - 1 \right) - \Lambda^T \Omega \quad (25)$$

where $\mathbf{F} = [\mathcal{F}^1, \mathcal{F}^2, \dots, \mathcal{F}^H]^T$, $\mathbf{1} = [1, 1, \dots, 1]^T$.

Assume $\hat{\Omega}$, $\hat{\zeta}$, $\hat{\Lambda}$ are the optimal solutions, according to the Karush-Kuhn-Tucker (KKT) conditions, for $\forall h$, we obtain that:

$$\begin{cases} \mathcal{F}^h + 2\eta \hat{\Omega}^h - \hat{\zeta} - \hat{\Lambda}^h = 0 \\ \hat{\Omega}^h \geq 0 \\ \hat{\Lambda}^h \geq 0 \\ \hat{\Omega}^h \hat{\Lambda}^h = 0 \end{cases} \quad (26)$$

the **Equation 26** can be re-formulated as:

$$\mathbf{F} + 2\eta \hat{\Omega} - \hat{\zeta} \mathbf{1} - \hat{\Lambda} = 0 \quad (27)$$

Following, we first solve the $\hat{\zeta}$ as:

$$\begin{aligned} \mathbf{F} + 2\eta \hat{\Omega} - \hat{\zeta} \mathbf{1} - \hat{\Lambda} &= 0 \\ \Rightarrow \hat{\zeta} \mathbf{1} &= \mathbf{F} + 2\eta \hat{\Omega} - \hat{\Lambda} \\ \Rightarrow \mathbf{1}^T \hat{\zeta} \mathbf{1} &= \mathbf{1}^T \mathbf{F} + 2\eta \mathbf{1}^T \hat{\Omega} - \mathbf{1}^T \hat{\Lambda} \\ \Rightarrow H \hat{\zeta} &= \mathbf{1}^T \mathbf{F} + 2\eta \mathbf{1}^T \hat{\Omega} - \mathbf{1}^T \hat{\Lambda} \\ \Rightarrow \hat{\zeta} &= \frac{\mathbf{1}^T \mathbf{F} + 2\eta \mathbf{1}^T \hat{\Omega} - \mathbf{1}^T \hat{\Lambda}}{H} \end{aligned} \quad (28)$$

Then we solve the $\hat{\Omega}$ as:

$$\begin{aligned} \mathbf{F} + 2\eta \hat{\Omega} - \hat{\zeta} \mathbf{1} - \hat{\Lambda} &= 0 \\ \Rightarrow 2\eta \hat{\Omega} &= \hat{\zeta} \mathbf{1} + \hat{\Lambda} - \mathbf{F} \\ \Rightarrow \hat{\Omega} &= \frac{1}{2\eta} \left(\hat{\zeta} \mathbf{1} + \hat{\Lambda} - \mathbf{F} \right) \\ &= \frac{1}{2\eta} \left(\frac{\mathbf{1}^T \mathbf{F} + 2\eta \mathbf{1}^T \hat{\Omega} - \mathbf{1}^T \hat{\Lambda}}{H} \mathbf{1} + \hat{\Lambda} - \mathbf{F} \right) \end{aligned} \quad (29)$$

Define

$$\hat{\Lambda}_{avg} = \frac{1}{H} \sum_{h=1}^H \hat{\Lambda}^h = \frac{\mathbf{1}^T \hat{\Lambda}}{H} \quad (30)$$

where $\hat{\Lambda}_{avg}$ is the average of $\hat{\Lambda}$, thus **Equation 29** can be rewritten as:

$$\begin{aligned} \hat{\Omega} &= \frac{1}{2\eta} \left(\frac{\mathbf{1}^T \mathbf{F} + 2\eta \mathbf{1}^T \hat{\Omega} - \mathbf{1}^T \hat{\Lambda}}{H} \mathbf{1} + \hat{\Lambda} - \mathbf{F} \right) \\ &= \frac{1}{2\eta} \left(\left(\frac{\mathbf{1}^T \mathbf{F}}{H} + \frac{2\eta}{H} \hat{\Lambda}_{avg} \right) \mathbf{1} + \hat{\Lambda} - \mathbf{F} \right) \\ &= \frac{1}{2\eta} \left(\left(\frac{\sum_{h=1}^H \mathcal{F}^h}{H} + \frac{2\eta}{H} \hat{\Lambda}_{avg} \right) \mathbf{1} + \hat{\Lambda} - \mathbf{F} \right) \end{aligned} \quad (31)$$

To this end, the optimal $\hat{\Omega}$ on h_{th} head can be formulated as:

$$\hat{\Omega}^h = \frac{1}{2\eta} \left(\frac{\sum_{h=1}^H \mathcal{F}^h}{H} + \frac{2\eta}{H} \hat{\Lambda}_{avg} + \hat{\Lambda}^h - \mathcal{F}^h \right) \quad (32)$$

Define $\mathcal{V}^h = \frac{\sum_{h=1}^H \mathcal{F}^h}{H} + \frac{2\eta}{H} \hat{\Lambda}_{avg} - \mathcal{F}^h$, we rewrite **Equation 32** as:

$$\hat{\Omega}^h = \frac{1}{2\eta} \left(\mathcal{V}^h - \hat{\Lambda}_{avg} + \hat{\Lambda}^h \right) \quad (33)$$

According to **Equation 26, 33**, we obtain that:

$$\hat{\Omega}^h = \begin{cases} \frac{1}{2\eta} \left(\mathcal{V}^h - \hat{\Lambda}_{avg} \right) & \text{if } \hat{\Omega}^h > 0 \\ 0 & \text{if } \hat{\Lambda}^h > 0 \end{cases} \quad (34)$$

Thus, the $\hat{\Omega}^h$ can be formulated as:

$$\hat{\Omega}^h = \frac{1}{2\eta} \max \left\{ \mathcal{V}^h - \hat{\Lambda}_{avg}, 0 \right\} \quad (35)$$

Define:

$$f(\Lambda_{avg}) = \frac{1}{H} \sum_{h=1}^H \max \left\{ \mathcal{V}^h - \Lambda_{avg}, 0 \right\} - \frac{2\eta}{H} \quad (36)$$

According to **Equation 23, 35, 36**, we obtain that:

$$\begin{aligned} f(\hat{\Lambda}_{avg}) &= \frac{1}{H} \sum_{h=1}^H \max \left\{ \mathcal{V}^h - \hat{\Lambda}_{avg}, 0 \right\} - \frac{2\eta}{H} \\ &= \frac{2\eta}{H} \sum_{h=1}^H \hat{\Omega}^h - \frac{2\eta}{H} \\ &= 0 \end{aligned} \quad (37)$$

so that we can use Newton method to solve this problem:

$$\Lambda_{avg(t+1)} = \Lambda_{avg_t} - \frac{f(\Lambda_{avg_t})}{f'(\Lambda_{avg_t})} \quad (38)$$

where $f'(\cdot)$ denotes the derivative function of $f(\cdot)$. t is the iteration number, means that we can get the optimal solution $\hat{\Lambda}_{avg}$ through t iterations. At last, we write the final solution as:

$$\hat{\Omega}^h = \frac{1}{2\eta} \max \left\{ \frac{2\eta}{H} + \frac{\sum_{h=1}^H \mathcal{F}^h}{H} - \mathcal{F}^h - \hat{\Lambda}_{avg}, 0 \right\} \quad (39)$$

where $\hat{\Lambda}_{avg}$ is computed from **Equation 38**.

B EXPERIMENTS

B.1 Influence of Unlabeled Samples

Semi-supervised few-shot learning utilizes the unlabeled samples to strengthen the classifier. The selected number has a significant influence on the final results, listed in **Figure 5**. With the increase of unlabeled instances, the proposed method has become more

effective. And the results start to saturate after 100 unlabeled samples.

B.2 Multi-Head Features Fusion

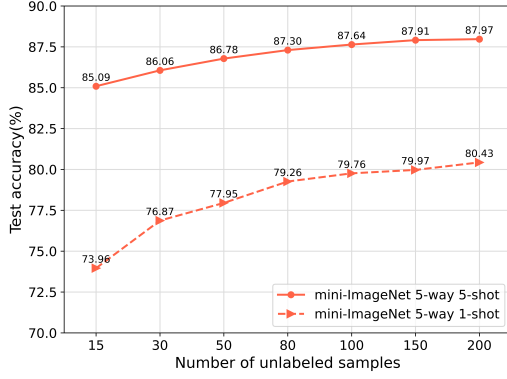
Besides SS-R-Fea and SS-M-Fea, we introduce Std-Fea and Meat-Fea (described in **Section 4.4**) to evaluate the proposed method further. We list the performances of more kinds of integrated ways on mini-ImageNet in **Table 5**. All the results are based on the transductive setting with a 5-way 1-shot case. We found that the more features are fused, the better the results are obtained. As examples, 5's ACC is higher than 1's and 2's; 11's ACC is higher than 1's, 2's, 5's, 6's, and 8's; 15's ACC is higher than all the others. The reason is that: The designed attention mechanism for fusing features can automatically adjust the impact of distinct features on the results and ensures that the fusion result is not worse than that of a single one. Besides, we conclude that if the to-be-fused features have similar performances, the final stacking result may have significant improvement, such as (3, 4, 10).

B.3 Influence of η in Attention Block

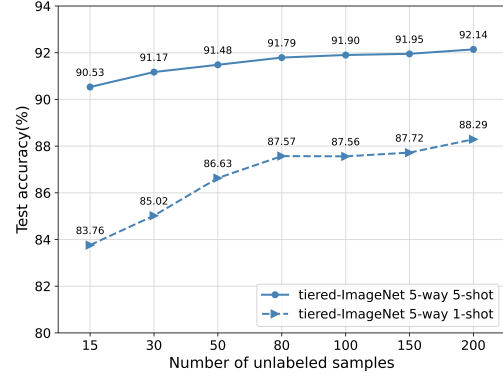
From **Equation 23**, we know that η is a parameter to influence the to-be-learned weights. For fairness and convenience, we have fixed η to 1.4 for all the experiments. Here, we list the results of other different η in **Figure 6**.

B.4 Confusion Matrix

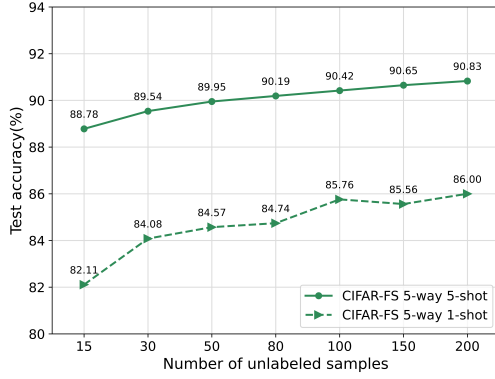
To further evaluate the impact of the "fusion", we illustrate the experimental results of each class. Specifically, we randomly select one episode (include 5 classes) on a 5-shot case, and show the corresponding confusion matrices of each head in **Figure 7,8,9,10**. Obviously, for a certain class, we obtain different results from different head features, while the proposed MHFC at least achieves similar performance as the best result of single-head. Thus, as the number of categories increases, the proposed method can naturally obtain more favorable results.



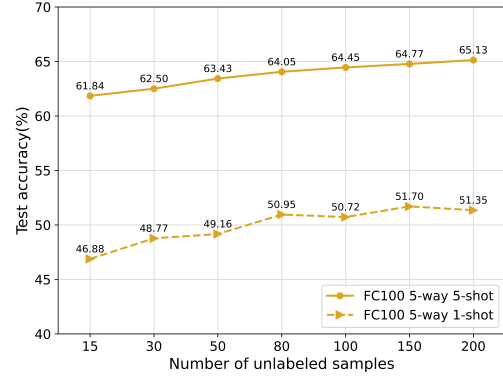
(a) mini-ImageNet



(b) tiered-ImageNet



(c) CIFAR-FS

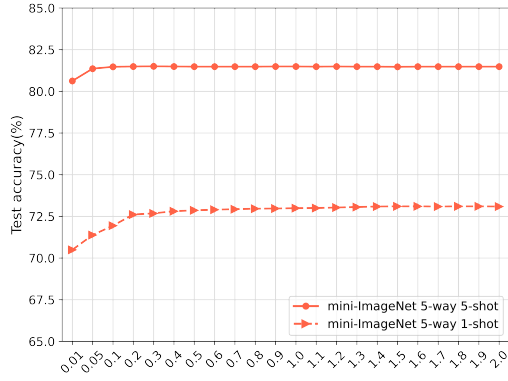


(d) FC100

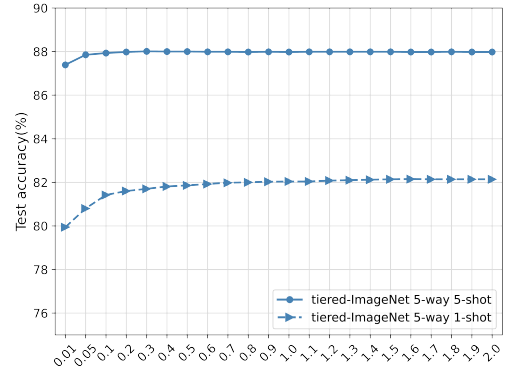
Figure 5: The comparison results of semi-supervised few-shot classification with varied unlabeled samples.

Table 5: Results of multi-head features fusion with the transductive setting on mini-ImageNet.

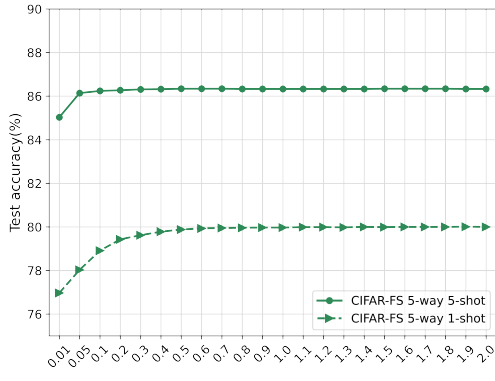
Features	1	2	3	4	5	6	7	8	9	10	11	12	13	14	15
Std-Fea [47]	✓				✓	✓	✓				✓	✓	✓		✓
Meta-Fea [2]		✓			✓			✓	✓		✓	✓		✓	✓
SS-R-Fea (ours)			✓			✓		✓		✓	✓		✓	✓	✓
SS-M-Fea (ours)				✓			✓		✓	✓		✓	✓	✓	✓
ACC	68.7	67.0	72.2	72.8	69.0	74.7	74.6	72.9	72.8	74.8	75.2	74.8	75.5	75.1	75.8



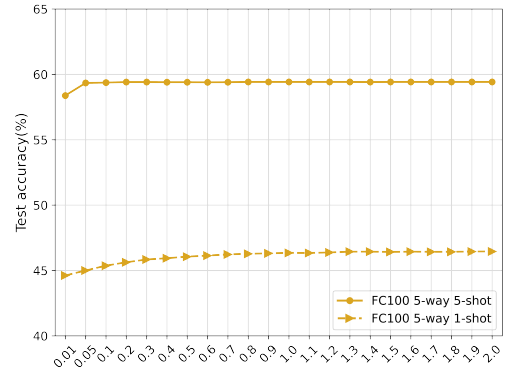
(a) mini-ImageNet



(b) tiered-ImageNet



(c) CIFAR-FS

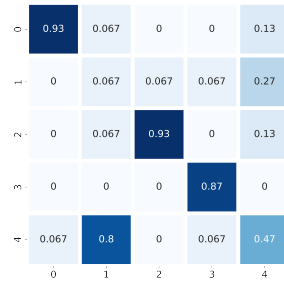


(d) FC100

Figure 6: Comparison results with different η on 5-way 1-shot case.



(a) SS-R-Fea



(b) SS-M-Fea



(c) Multi-Head-Fea

Figure 7: Confusion matrices on mini-ImageNet with inductive setting.

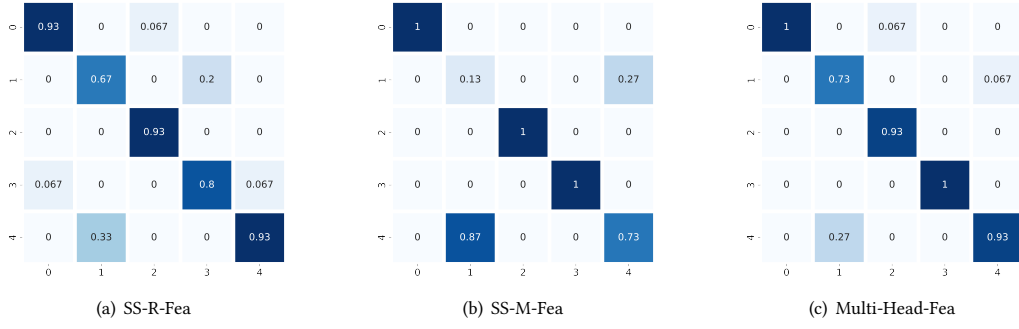


Figure 8: Confusion matrices on tiered-ImageNet with inductive setting.

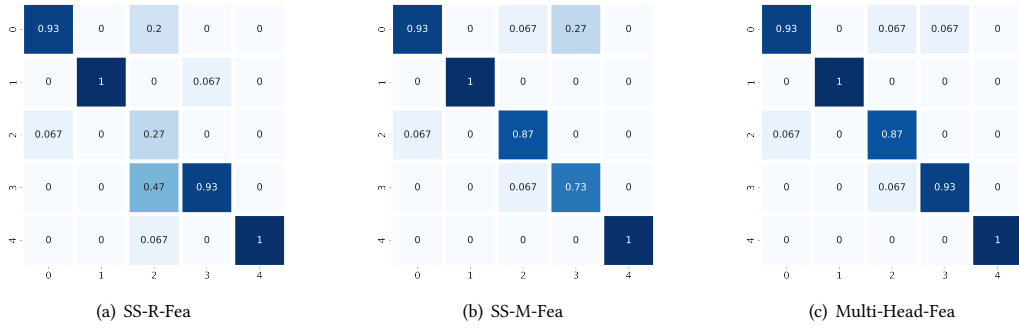


Figure 9: Confusion matrices on CIFAR-FS with inductive setting.



Figure 10: Confusion matrices on FC100 with inductive setting.